Climatic cycles as expressed in sediments of the PROMESS1 borehole PRAD1-2, central Adriatic, for the last 370 ka: 1. Integrated stratigraphy

Andrea Piva

ISMAR, Consiglio Nazionale delle Ricerche, Via Gobetti 101, I–40129 Bologna, Italy (andrea.piva@bo.ismar.cnr.it)

Alessandra Asioli

IGG, Consiglio Nazionale delle Ricerche, Via Giotto 1, I–35100 Padova, Italy

Ralph R. Schneider

Institut für Geowissenschaften, Christian–Albrechts–Universität zu Kiel, Ludewig–Meyn–Str. 10, D–24118 Kiel, Germany

Fabio Trincardi

ISMAR, Consiglio Nazionale delle Ricerche, Via Gobetti 101, I–40129 Bologna, Italy

Nils Andersen

Leibniz Laboratory for Radiometric Dating and Stable Isotope Research, CAU Kiel, Max–Eyth–Str. 11, D–24118 Kiel, Germany

Elena Colmenero-Hidalgo

Departamento de Geología, Facultad de Ciencias, Universidad de Salamanca, E–37008 Salamanca, Spain

Bernard Dennielou

Ifremer, Département des Géosciences Marines, BP70, F–29280 Plouzané Cedex, France

José-Abel Flores

Departamento de Geología, Facultad de Ciencias, Universidad de Salamanca, E–37008 Salamanca, Spain

Luigi Vigliotti

ISMAR, Consiglio Nazionale delle Ricerche, Via Gobetti 101, I–40129 Bologna, Italy

[1] A multiproxy integrated chronological framework, based on oxygen and carbon stable isotope stratigraphy, biostratigraphy (foraminifera and nannoplankton bioevents and foraminifer assemblage-based climate cyclicity), magnetostratigraphy, sapropel stratigraphy, and ^{14}C AMS radiometric dates, has been achieved for borehole PRAD1-2, collected in 185.5 m water depth in the central Adriatic. This work was carried out within the European Community project Profiles across Mediterranean Sedimentary Systems (PROMESS1). The 71.2 m long borehole spans a time interval between late MIS 11 and MIS 1 (the last 370 ka), showing a chronological resolution of 500 and 250 years per cm during interglacial and glacial intervals, respectively. At present, this record is the most expanded and continuous marine record available for the Adriatic Basin. Several orbital cycles can be recognized in the PRAD1-2 record: the 100 ka glacial-interglacial fluctuations and the 23 ka precession-related cycles, which in turn control the deposition of sapropel layers. An integrated analysis of short-term oscillations within the Last Glaciation interval

(MIS 4–MIS 2) allowed the identification of the Adriatic signature of Dansgaard-Oeschger events, showing the potential to achieve a more refined chronostratigraphic framework for the top part of the PRAD1-2 record. Finally, the age model obtained by this study allowed the chronological integration of the main foraminifera bioevents detected in the borehole as well as of the volcanoclastic layers present in the upper part of the record. Despite its proximal location, PRAD1-2 presents a continuous record and shows the potential to be consistently correlated both with deep-sea and continental records in the Mediterranean region and beyond.

1. Introduction

[2] The European Community-funded Profiles across Mediterranean Sedimentary Systems (PROMESS1) project was the first attempt of scientific drilling through the Mediterranean margins, with the aims of (1) deciphering the impact of global sea level change on sequence architecture of shelf and slope deposits and (2) resolving past climate change at century to decadal-scale resolution over the last ∼500 ka. The project focused on investigating two complementary deltaic margins, the NW Mediterranean (fed by the Rhone and Catalan-Languedocian river system) and the Adriatic (fed by the Po and Apennine river system) by coring two boreholes in each location. The sediment sequences in both areas have high sedimentation rates and good sequence preservation but show contrasting regional tectonic settings. The possibility of extensively correlating shelf and slope domains provides the opportunity to constrain chronologically distinctive changes within the rather thick shelf successions for paleoenvironmental reconstructions during the last four glacial cycles.

[3] Sedimentary deposits on Quaternary continental margins have the potential of recording the impact of climate change occurring on several orders of cyclicity [*Sydow and Roberts*, 1994; *Skene et al.*, 1998]. Where the sediment flux is sufficiently high the Milankovitch-driven cyclicity appears punctuated by higher-frequency oscillations at millennial to century-scale, including abrupt climatic change. However, extracting paleoenvironmental and paleoceanographic information from shallow continental-margin settings is per se a challenge because in these settings the shallow depth and the vicinity to the sediment sources may introduce a greater complexity to the stratigraphic record compared to equivalent records in the deep sea, particularly during glacial intervals when more sediment reached the upper slope. In the Adriatic region, the longest continuous and high-resolution record is borehole VE-1 [*Massari et al.*, 2004], drilled in the Venice lagoon (500 km north of the central Adriatic area studied in this work) and reaching upper Pliocene sediments. At this site glacial-interglacial cycles of the last 400 ka are represented by repeated oscillations from alluvial plain to inner shelf environments. In addition, *Amorosi et al.* [1999, 2004] published a detailed stratigraphy of several boreholes reaching Marine Isotope Stage (MIS) 7c on the coastal plain near Ravenna. At this site, alluvial plain environments characterize all glacial intervals while coastal environments record interglacial intervals like MIS 5.5. Central Adriatic PRAD1-2 borehole, analyzed in this paper, represents the first attempt to study a continuous marine record for the last ∼400 ka at a key site influenced by the same catchment but also impacted by the main water masses affecting the eastern Mediterranean circulation, such as the Levantine Intermediate Water (Figure 1).

[4] This paper aims at providing the chronostratigraphic framework for borehole PRAD1-2 in
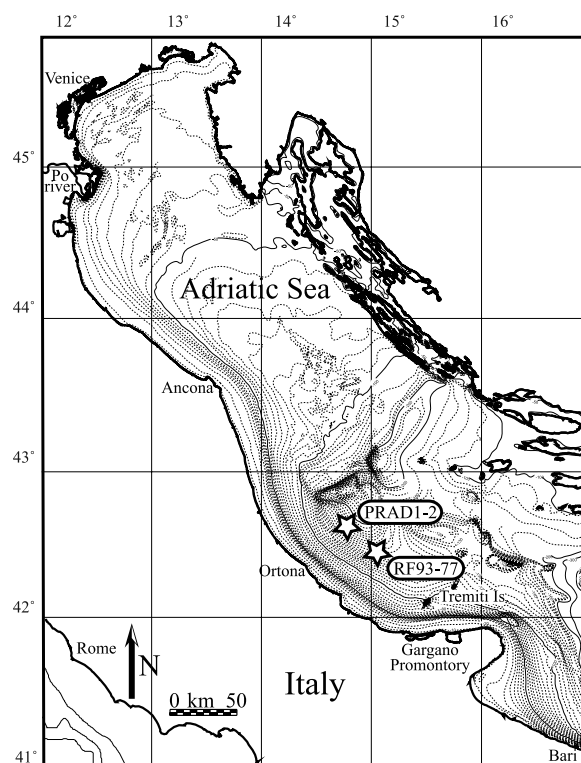
Figure 1. Location of borehole PRAD1-2 on the central Adriatic upper slope. Reference core RF93-77 is located slightly to the south in a similar water depth [*Guillizzoni and Oldfield*, 1996].

the central Adriatic shallow slope basin integrating magnetostratigrapy with bioevents and stable isotope stratigraphies. This chronological framework forms the base for three companion papers focusing on the paleoceanographic reconstruction in the context of the central Mediterranean [*Piva et al.*, 2008], the geo-history of PRAD1-2 borehole (F. Trincardi et al., manuscript in preparation, 2008) and the sequence stratigraphic implications including the partitioning of sedimentary sequences in highstand, low-stand and transgressive deposits (D. Ridente et al., The composite record on fourth- and fifth-order glacioeustatic cycles during the last 400 ka in the central Adriatic Sea: Margin growth and sequence architecture, submitted to *Geochemistry, Geophysics, Geosystems*, 2007; hereinafter referred to as Ridente et al., submitted manuscript, 2007).

2. Materials and Methods

[5] PRAD1-2 borehole was located in the Mid-Adriatic Deep, (LAT 42°40′34.7826″N; LONG 14°46′13.5565″E) in 185.5 m water depth (Figure 1). The coring device on board R/V *Bavenit*, a geotechnical vessel owned by FUGRO, provided a continuous sediment core of 71.2 m, with a recovery of 99.96%. This is the longest marine record of substantially undisturbed sediment available for the Adriatic Basin. The borehole consists of 89 cores (sections), each of which is about 75–80 cm long on average and 6 cm in diameter. After splitting, one half core was stored as archive, whereas the working half has been sampled for multiple analyses (micropaleontology and macropaleontology, sedimentology, magnetostratigraphy, geochemistry and sediment properties). Materials and methods used for the chronostratigraphic framework include foraminifera and calcareous nannoplankton stratigraphies, oxygen and carbon stable isotope profiles, radiocarbon dating as well as sediment magnetic properties and color reflectance and elemental composition profiles (X-ray fluorescence (XRF) analysis).

2.1. Foraminifera

[6] A total of 784 subsamples was taken in 2-cm slices (equivalent to about 28–30 cc), with a typical sampling interval of 10 cm. The sampling distance was reduced where a higher-resolution record was required. All the subsamples were dried in the oven at 50°C and weighed. Subsequently the samples were washed and sieved through a 63 μm mesh and dried again at 50°C. The samples were split into aliquots using a Jones microsplitter and a number of aliquots was counted to reach at least 300 planktic and 300 benthic specimens. The total number of specimens of each species for each sample was estimated after counting. The counting was performed on the fraction >106 μm, to avoid juvenile specimens. However, the fraction <106 μm was always checked, in order to identify those specimens which can pass the mesh because of an elongated shape of their shell (such as *Fursenkoina*), or because of the small size of their adult stage (e.g., *Epistominella*). Some planktic species or morphotypes were lumped together according to the following scheme: *Globigerinoides* ex gr. *ruber* includes *Globigerinoides ruber* and *Globigerinoides elongatus*; *Orbulina* includes both *Orbulina universa* and *Orbulina suturalis*; *Globigerinoides sacculifer* comprehends *Globigerinoides trilobus, Globigerinoides sacculifer* and *Globigerinoides quadrilobatus* (in the sense of *Hemleben et al.* [1989]). Taxa are quantified as percentages of the total number of planktic and benthic foraminifera, respectively, while the con-

centration is reported as the number of specimens per gram of dry sediment. The ecological requirements of planktic species, for instance the grouping of warm and cold species, are well known and refer, e.g., to *Pujol and Vergnaud Grazzini* [1995], *Hemleben et al.* [1989], and *Sen Gupta* [1999].

2.2. Calcareous Nannoplankton

[7] Samples of about 1 cc of sediment were extracted from the lowermost parts of the cores immediately after their arrival on board. This material was taken from the core centre in order to avoid contamination by sediment from other depths, drilling mud or external material accumulated at the edge of the PVC liner. Smear slides were examined under a light microscope at around $\times1000$ magnification under both direct and cross-polarized light. Observations across more than 100 visual fields were performed, this in order to search for age marker taxa in critical stratigraphic intervals. Additionally, approximately two thirds of those smear slides were reexamined and more than 300 coccoliths were identified and counted in each slide in order to estimate the relative abundances of the different taxa in a semiquantitative fashion. A separate count of the reworked nannofossils (identified as belonging to Mesozoic and Tertiary taxa, extinct in the Quaternary) present in the same visual fields was also carried out, and the percentage of those particles in relation to the number of coccoliths was calculated. During the counting, forms of *Emiliania huxleyi* larger and smaller than 4 μm were separated, following *Colmenero-Hidalgo et al.* [2002] and forms of the genus *Gephyrocapsa* were divided into size groups, with the exception of *Gephyrocapsa caribbeanica*, following *Flores et al.* [1999].

2.3. Oxygen and Carbon Stable Isotopes

[8] The analyses were performed on the $CaCO_3$ of shells of selected monospecific foraminifera specimens. In particular, twenty specimens (on average) of *Globigerina bulloides* (planktic) and *Bulimina marginata* (benthic) were picked from the size fraction >180 μm. These two species were chosen because they are present in sediments throughout the borehole. The analyses were performed at the Leibniz Laboratory for Radiometric Dating and Stable Isotope Research, CAU Kiel, Germany, by using the Kiel automated carbonate preparation device, connected to a MAT 251 mass spectrometer. In the Kiel device, CO_2 is liberated from the carbonate samples by adding several drops of 100% phosphoric acid individually to each sample. The reaction with phosphoric acid in evacuated sample vials takes place at a constant temperature of 75°C. The reaction time is about 4 min. The liberated CO_2 and the H_2O, which is also produced during the reaction, are afterward quantitatively frozen in a so-called multiloop with the help of liquid nitrogen (about -196°C), and subsequently heated to a temperature of about -55°C; at this temperature H_2O is still frozen in the multiloop, but all CO_2 is liberated again. Each sample gas is measured ten times (in a succession of reference gas, sample gas, reference gas, sample gas, etc.). The external error of each measurement is better than 0.04‰ (^{13}C) and 0.06‰ (^{18}O).

2.4. Radiometric Datings

[9] ^{14}C AMS datings were performed on benthic monospecific samples (*Elphidium crispum* or *Hyalinea balthica*) at the Poznan Radiocarbon Laboratory, Poland, by using specimens from the size fraction >250 μm. Ages were calibrated using two calibration programs: the online Calib 5.0.2 Radiocarbon Calibration Program [*Stuiver and Reimer*, 1993] for radiocarbon ages B.P. younger than 20,000 years (marine sample = 100%, Calibration data set: Marine04 ^{14}C according to *Hughen et al.* [2004]) and the recently published online calibration program by *Fairbanks et al.* [2005] for ages older than 20,000 years (http://radiocarbon. LDEO.columbia.edu) (Table 1).

[10] Calibration with Calib 5.0.2: in order to calculate the ΔR (reservoir), two sites on the western side of the Adriatic were selected from the Calib 5.0.2 database to be used in the calibration: one from the northern Adriatic (Rimini, 487 years) and another from the southern Adriatic (Barletta, 483 years), avoiding data from Dalmatia and Croatia (Rovigne) (262 and 254 years, respectively). The higher reservoir age of the western Adriatic flank likely reflects the river input of older carbon-rich sediments. We assume that, during the last climate cycle at least, the area where PRAD1-2 borehole was recovered was mostly influenced by the western Adriatic catchment area. The calculated weighted mean ΔR value is 135.8 years with a standard deviation of 40.8 years.

[11] In order to calculate the marine effect to be used in the online program of *Fairbanks et al.* [2005], the same two sites from the Adriatic were selected from *Fairbanks et al.* [2005], *Butzin et al.* [2005], and L. Cao et al. (The marine radiocarbon reservoir age, manuscript in preparation, 2007) for

Table 1. Calibrated Ages According to the Calib5.0.2 ^{14}C Dating Program and to the *Fairbanks et al.* [2005]^{14}C Dating Program[a]

Lab. N.	Sample	Depth, mbsf	Material	^{14}C Age, B.P.	Cal. Age, Years B.P.	Std. Dev.	Calibration Method
Poz-16129	PRAD1-2 S8 cm 40−42	5.976	*E. crispum*	14930 ± 90	16760−17776		Calib 5.0.2
Poz-16130	PRAD1-2 S10 cm 60−62	7.8	*E. crispum*	16530 ± 100	18968−19411		Calib 5.0.2
Poz-16131	PRAD1-2 S17 cm 60−62	13.4	*E. crispum*	24130 ± 150	28435	178	*Fairbanks et al.* [2005]
Poz-16132	PRAD1-2 S17 cm 60−62	13.4	*H. balthica*	23390 ± 150	27654	181	*Fairbanks et al.* [2005]
Poz-17321	PRAD1-2 S19 cm 40−42	14.8	*E. crispum*	28960 ± 270	33450	482	*Fairbanks et al.* [2005]
Poz-17320	PRAD1-2 S21 cm 40−42	16.386	*H. balthica*	36700 ± 600	41626	376	*Fairbanks et al.* [2005]

[a] The Calib5.0.2 ages are expressed as ranges (2σ), and the *Fairbanks et al.* [2005] ages are expressed as mean values (1σ).

the reservoir output. The calculated reservoir is 262 and 254 years for Rimini and Barletta sites, respectively. Then, a mean age of 258 years was used for the calibration of PRAD1-2 (^{14}C age minus 258 = ^{14}C age to be calibrated).

2.5. Magnetic Properties

[12] U-channels were extracted from the working half of the 89 cores of PRAD1-2 borehole. A full paleomagnetic study of the U-channel was carried out at the University of California Laboratory in Davis, using an automated 2G Enterprises cryogenic magnetometer. Paleomagnetic and rock-magnetic investigations were carried out at 1 cm steps as follows: (1) The Natural Remanent Magnetization (NRM) was measured through an alternating field (AF) demagnetization in 5 steps up to 50−60 mT, depending on the coercivity of the sediment. On the basis of preliminary tests, the applied peak fields were deemed to be sufficient to reduce the NRM at about 10% of the initial value and to remove secondary overprints. (2) An anhysteretic remanent magnetization (ARM) (90 mT AF + 0.1 mT direct current (DC) field) was imparted to the sediment and demagnetized in 3 steps (20−30−40 mT), representing most of the magnetic coercivity spectrum. (3) An isothermal remanent magnetization (IRM) at 1 T was applied to the sediment. The U-channels were demagnetized in 6 steps up to 60 mT.

2.6. Color Reflectance

[13] Spectral color was measured at IFREMER (Brest) by means of a Spectrophotometer Minolta CM-508. Data from 400 to 700 nm wavelength (measured with a wavelength interval of 10 nm) were obtained every two centimeters. We use both the color reflectance (to uniform to the method used by *Lourens* [2004] for sapropel identification) and the lightness (L*) from the CIE 1976 L*a*b*

color space; low values indicate dark sediment and high values light sediment.

2.7. XRF Data

[14] X-ray fluorescence (XRF) data were acquired with the Cortex XRF-scanner [*Jansen et al.*, 1998] at the Bremen core repository. The scanner produces semiquantitative counts of the elemental chemical composition (K, Ca, Ti, Fe, Sr) of the sediment. Measurements were performed on split core at 2 cm intervals. Intrinsic sediment heterogeneity (grain size, water content) does not meet requirements of conventional laboratory XRF analysis and the reliability of the results also depends on disturbances (unevenness, cracks) on the scanned surface [*Croudace et al.*, 2006; *Richter et al.*, 2006]. Consequently, erroneous data were removed by hand. As this instrument cannot precisely measure Al, Ti was used for normalization to the alumino-silicate detrital phase.

3. Chronostratigraphic Framework

[15] The chronological framework is presented in two steps: the first is based on stratigraphic proxies, including stratigraphy based on oxygen and carbon stable isotopes, magnetostratigraphy and the main microfaunistic bioevents, constrained for the upper part of the borehole by the available radiocarbon dates (Figure 2). The second is a fine-tuning exercise based on the recognition of paleoenvironmental ''events'' as recorded by quantitative changes in the foraminifera assemblages and associated stable isotope excursions in their shells which can be correlated to the eastern Mediterranean sapropels (Figures 5 and 6 in section 4). In addition, the Dansgaard-Oeschger events were identified during the last ∼80 ka (Figure 7 in section 5). All the obtained age control points are summarized in Table 2 in section 6, concur in producing a refined age model (Figures 8 and 9 in section 6) and provide the calibration of the main
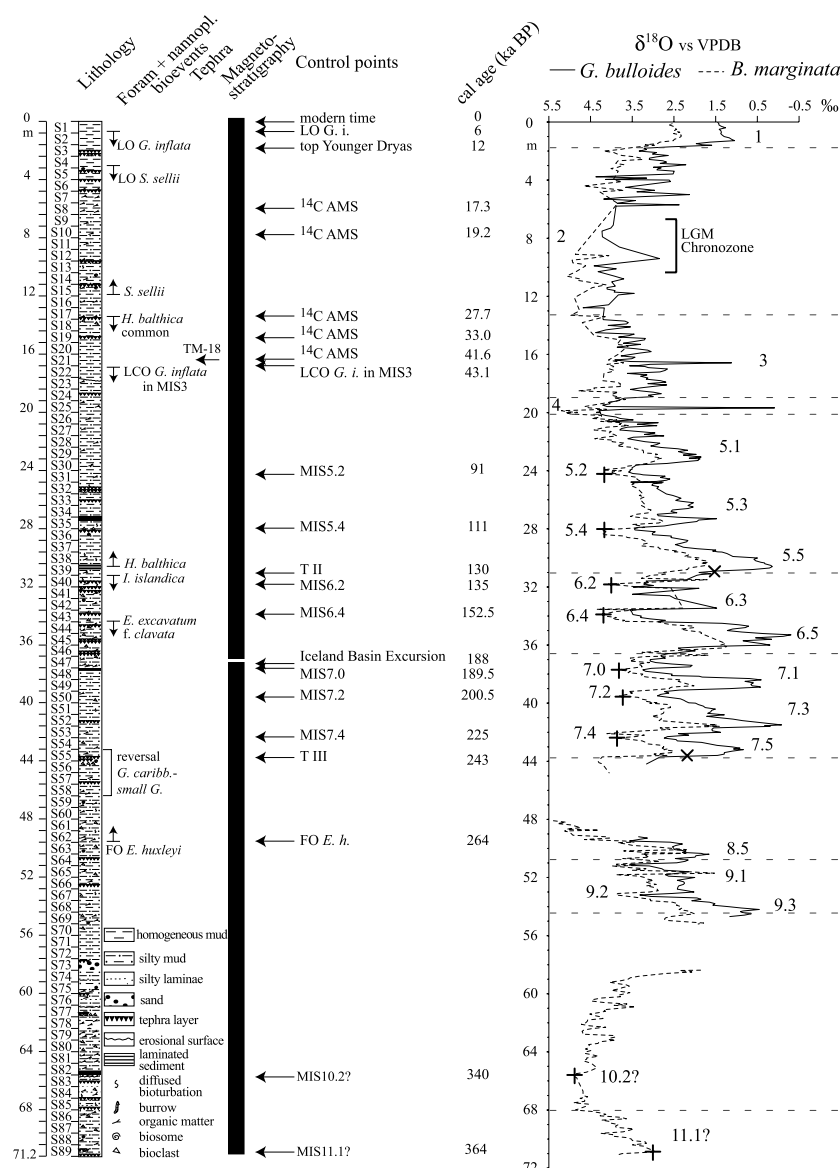
Figure 2. Stratigraphic scheme for PRAD1-2, based on the stable oxygen isotope stratigraphy, magnetostratigraphy, radiocarbon dates, and identification of bioevents. "X" symbols identify the control points taken on the Termination midpoints (according to *Lisiecki and Raymo* [2005]); plus ("+") symbols mark control points corresponding to dated substages relative maxima/minima values (according to *Martinson et al.* [1987] and *Bassinot et al.* [1994]).

foraminifera bioevents recognized in PRAD1-2 record (Table 3 in section 7).

3.1. Isotope Stratigraphy

[16] Two $\delta^{18}O$ records, obtained from the planktic foraminifer *G. bulloides* and from the benthic foraminifer *B. marginata*, show very consistent (subparallel) trends, albeit the latter is systematically shifted toward higher values (Figure 2). The $\delta^{18}O$ record of *G. bulloides* allows reconstruction of the most significant stratigraphic events (Marine

Isotope Stages: MIS), showing abrupt shifts from highest (~4‰) to the lowest values (less than 0.5‰) at approximately 2, 32, 44 m below seafloor (mbsf). These major shifts are paralleled by similar shifts in the benthic $\delta^{18}O$ record (typically between 5 and 2.5‰) and can be ascribed to isotopic Terminations at the end, respectively, of MIS 2, MIS 6 and MIS 8. The planktic-based isotopic record is not continuous through certain intervals. The *G. bulloides* $\delta^{18}O$ record reveals significant gaps between 5 and 7 m, 44 and 49 m, and in the lowermost interval (18 m) of the core. These

intervals represent glacial periods in correspondence of MIS 2, MIS 8, and probably MIS 10, characterized by very high values in the benthic $\delta^{18}O$ record and a cold-water planktic assemblage (if present). The extreme scarcity or absence of plankton in these intervals occurred during periods of lowered eustatic sea level, when the thickness of the water column was reduced limiting planktic foraminifera growth. However, the combined planktic and benthic isotope records allowed recognition of subordinate climatic oscillations, such as the cold and warm isotopic substages within the major interglacial intervals MIS 5, MIS 7 and MIS 9 (Figure 2).

[17] In detail, the $\delta^{18}O$ record of *G. bulloides* displays scattered abrupt spikes (with excursions up to 3‰ toward lighter values) in the upper 6 m of the core. This evidence possibly indicates diluted surface water salinity over short-lived intervals of increased run off from the Po low-stand delta on the NW edge of the central Adriatic basin, which was markedly reduced in extent and fresh-water dominated [*Cattaneo and Trincardi*, 1999; *Asioli et al.*, 2001]. Moreover, the warm water component of the planktic assemblage is almost absent in this interval; therefore this evidence does not support a strong temperature effect in the $\delta^{18}O$ record.

[18] The stratigraphic interpretation of the lowest part of the core, below 55 mbsf, is more problematic. For this interval, predating the base of MIS 9, only a benthic $\delta^{18}O$ record is available and presents the most positive values (+4.7‰) between 65.5 and 68 mbsf. We have ascribed this interval to MIS 10.2, although the exact positioning of the correspondent control point in the age-depth model is still uncertain. Above 65.5 mbsf the oxygen composition gradually decreases of about +3.7‰ with small fluctuations in amplitude, culminating in a strong shift to +1.7‰ at 58.2 mbsf, comparable to the ones during MIS 9.3. Below 68 mbsf the benthic $\delta^{18}O$ values reach about +3‰, a value comparable to average benthic values typical of warm intervals, such as MIS 9, MIS 5.3, MIS 5.1 and MIS 3. Therefore the bottom of the borehole is ascribed to MIS 11.1, under the assumption of the continuity of the stratigraphic record.

[19] Both the planktic and benthic isotopic records allow recognition of the major Terminations (T I, T II and T III): midpoints of T II and T III have been taken as control points for the age model (referring to *Lisiecki and Raymo* [2005]). These midpoints are marked by a "X" in Figure 2. We did not include an age for the midpoint of Termination I (14 ka, according to *Lisiecki and Raymo* [2005]) in the age-depth model because the literature provides a higher number of control points (e.g., the base of the Bolling-Allerod, the top of the Younger Dryas) for this time interval in the central Adriatic Basin [*Asioli*, 1996; *Asioli et al.*, 1999; *Ariztegui et al.*, 2000]. These control points mainly rely on bioevents dated in other cores and recognized in PRAD1-2 record. Nine additional control points (marked by a "+" in Figure 2) were included for the interval older than MIS 5.1. Seven are based on the ages of glacial stages and cold substages of the SPECMAP standard isotope curve [*Martinson et al.*, 1987], while the ages correspondent to MIS 10.2 and MIS 11.1 are from *Bassinot et al.* [1994].

3.2. Calcareous Nannoplankton Biostratigraphy

[20] The preliminary semiquantitative analysis of calcareous nannoplankton assemblages was carried out onboard R/V *Bavenit* during the PROMESS1 cruise, by means of smear slides. The preservation of coccoliths is moderate to good and specimens are generally abundant. Taxa belonging to the genus *Gephyrocapsa* and the species *Emiliania huxleyi* dominate the nannoplankton assemblage. The amount of reworked nannofossils (i.e., those identified as belonging to Tertiary and Mesozoic taxa, as indicated before) in PRAD1-2 record shows several peaks up to 80% of the total of counted coccoliths, especially at 5–10 mbsf (MIS 2), 33 mbsf (MIS 6), 46 mbsf (MIS 8) and 60 mbsf (MIS 10). However, despite the recognized importance of the reworked component, some key biostratigraphic events help refining the stratigraphy of the borehole:

[21] 1. Few specimens of *Pseudoemiliania lacunosa* were identified at the very bottom of the borehole, but the extensive reworking in these samples makes their origin uncertain. Therefore the age of the base of the borehole is younger than the Last Occurrence (LO) of *P. lacunosa* (in the sense of *Rio et al.* [1990], end of Nannofossil Zone NN19 of *Martini* [1971]) which is usually established around 460 ka.

[22] 2. The First Occurrence (FO) of *E. huxleyi* [*Rio et al.*, 1990] was identified at around 49.5 mbsf (bottom of section 62). *Thierstein et al.* [1977] established an age of 268 ka (top of MIS 8) for this event. In our age model we introduce the astronomically calibrated age of 264 ka for this

event, according to *Lourens* [2004]. This age is consistent with the stable isotope stratigraphy.

[23] 3. A reversal in the dominance of the assemblage from *G. caribbeanica* to the group of small *Gephyrocapsa* is recorded between 46.33 and 43.17 mbsf (lowermost parts of sections 58 to 54), close to the FO of *E. huxleyi* and is identified as equivalent to the one commonly observed in Atlantic records during MIS 8 [*Hine and Weaver*, 1998]. This event has been dated between 260 and 245 ka (i.e., top of MIS 8) off the Azores Islands [*Villanueva et al.*, 2002].

3.3. Foraminifera Biostratigraphy

[24] The study of foraminiferal assemblages started with a semiquantitative analysis of the entire borehole sequence defining a preliminary overall stratigraphic trend and the characterization of the depositional environments. On the basis of the indications from this preliminary survey, 307 selected samples have been quantitatively analyzed. The interval between 60 and 68 mbsf, ascribed to MIS 10 (on the basis of the isotope stratigraphy presented above), was analyzed at low resolution, because the semiquantitative study indicated a relatively homogeneous foraminifer assemblage without frequent significant variations. Foraminifera results are here used for stratigraphic purpose in terms of bioevents and climate cyclicity.

[25] The main planktic foraminifer bioevent is the LO of *Globorotalia inflata* at 6 ka B.P., approximating the mid-Holocene and it is a well-constrained biostratigraphic event for the central Adriatic [*Jorissen et al.*, 1993; *Asioli*, 1996; *Ariztegui et al.*, 2000; *Asioli et al.*, 1999, 2001].

[26] Moreover, the long time interval spanned by the borehole allowed the recognition of the following planktic and benthic foraminifera bioevents, some of them already recorded in literature but with a very uncertain associated age: (1) Last Common Occurrence (LCO) of *G. inflata* at 16.9 mbsf within MIS 3; (2) LO of *Sigmoilina sellii* at 3 mbsf (according to *Jorissen et al.* [1993], this event, dated at ~12.7 ka B.P. (^{14}C age) approximates the base of the Bolling interval [*Asioli*, 1996]); (3) entry of *S. sellii* at ~12 mbsf dated at 15.3 ka B.P. (^{14}C age), according to *Jorissen et al.* [1993]; (4) LCO of *Hyalinea balthica* at 14 mbsf (new bioevent for the central Adriatic biostratigraphy); (5) entry of *H. balthica* at ~30.6 mbsf (new bioevent for the central Adriatic biostratigraphy); (6) LO of *Islandiella islandica* at 31.2 mbsf (new bioevent for

the central Adriatic biostratigraphy); (7) LO of *Elphidium excavatum* forma *clavata* at 34.4 mbsf (MIS 6) [*Borsetti et al.* 1995].

[27] The recognition of significant variations in the assemblages of planktic and benthic foraminifera shows periodic changes in the depositional environment including warm-cold oscillations and accompanying variations of paleodepth); these variations were compared and integrated with the isotope stratigraphy. The succession of warm and cold intervals shows alternation of interglacial periods, characterized by abundant planktic foraminifera, typical of warm climate conditions (*Globigerinoides* ex gr. *ruber*, *Orbulina*, *Zeaglobigerina rubescens, Globigerinoides sacculifer*, *Globigerinella* spp) and glacial intervals, showing either scarce planktic content, dominated by cold water foraminifera (*Globigerina bulloides*, *Globigerina quinqueloba* and in some case *Neogloboquadrina pachyderma*), or intervals void of plankton. The cold water assemblage allows recognition of four well-defined glacial intervals (respectively between 10 and 20 mbsf, 31 and 38 mbsf, 44 and 49 mbsf, 55 and 68 mbsf), in good agreement with the isotope stratigraphy. In the lowermost part of the core, between 69 mbsf and the base of the borehole, the foraminifera assemblage indicates relatively warm conditions and a slightly deeper depositional environment, compared to the overlaying sections (reduced occurrence of *Elphidium* + *Ammonia* shelf benthic assemblage, in favor of species indicating upper slope facies, Figure 3); concurrently, the benthic oxygen isotope curve shows lower values, strongly suggesting that the borehole reached the upper part of the MIS 11 interglacial.

[28] Planktic foraminifera are scarce or absent during glacial intervals because the water column in the shallow and semienclosed Mid-Adriatic Deep was substantially reduced when global sea level fell. The glacial signal is however picked by the benthic assemblage, which changed species composition during different paleodepth conditions. While interglacial intervals are characterized by an outer shelf to upper slope foraminiferal assemblage (*Uvigerina peregrina*, *Uvigerina mediterranea*, *Gyroidinoides* spp, *Cibicidoides pachyderma*, *Bulimina* ex gr. *marginata*, *Brizalina spathulata-catanensis*, *Trifarina angulosa*, *H. balthica*, *Cassidulina laevigata carinata*) [*Jorissen*, 1987, 1988; *de Stigter et al.*, 1998; *Murray*, 2006], glacial intervals show a marked shift toward middle to inner shelf environments (assemblages
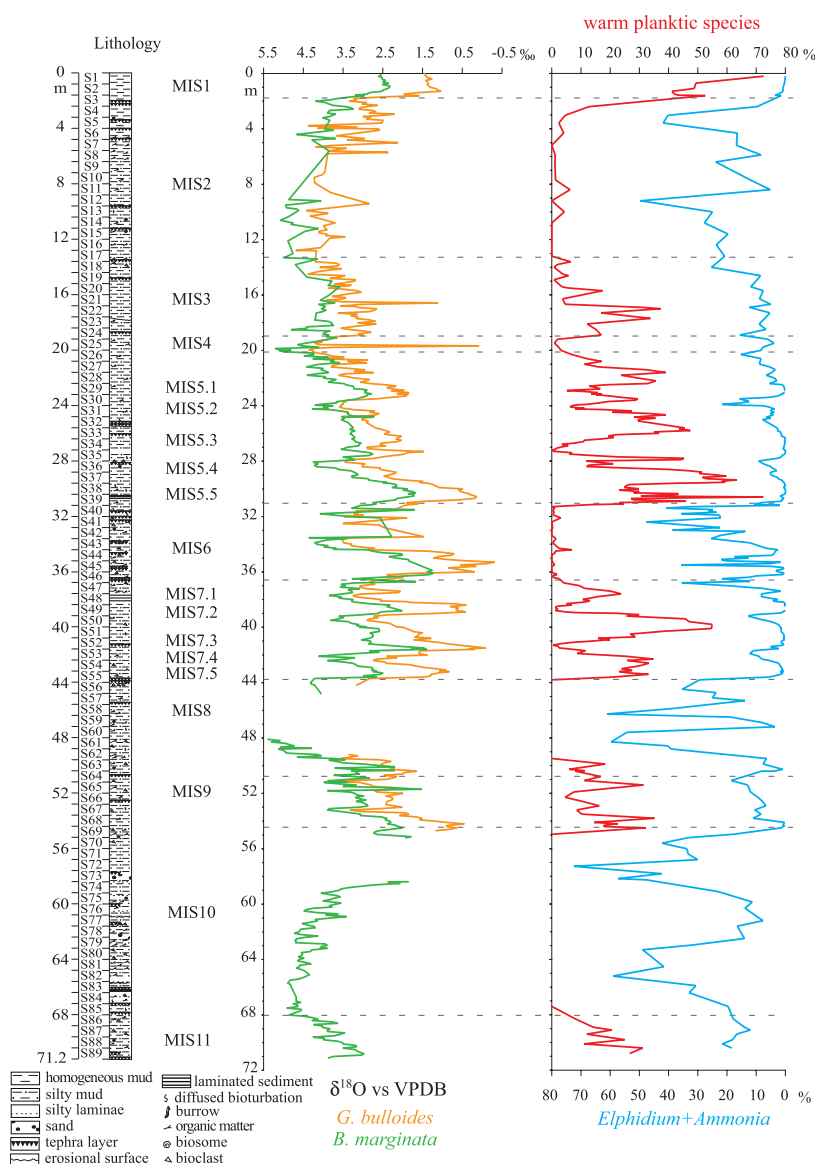
Figure 3. Cyclicity of PRAD1-2 as recorded by changes in stable oxygen isotope values (on both benthic and planktic foraminifera), abundance of warm- and cold-climate foraminifera associations, and abundance of proximality indicators.

dominated by *Elphidium* spp, *Ammonia perlucida*, *Nonion* spp, *Bulimina* ex gr. *marginata*, *C. laevigata carinata*, *I. islandica*) [*Jorissen*, 1987, 1988; *Van der Zwaan and Jorissen*, 1991; *Murray*, 2006]. These oscillations in the paleo-depth can be represented by the *Elphidium + Ammonia* curve (Figure 3). In fact, studies of the modern benthic foraminifera distribution in the Adriatic show that these two taxa reach their highest abundance in the inner shelf environment (less than 25 m, according to *Jorissen* [1987, 1988]). Therefore the modern distribution of these two taxa is here used as proxy of the inner shelf environment, and

consequently of relative sea level regression phase.

3.4. Magnetostratigraphy and Magnetic Properties

[29] After AF cleaning the NRM directions exhibit a constant normal polarity for all the sections, so that the borehole can be completely ascribed to the Brunhes Normal-polarity Magnetozone. Two short intervals with reverse polarity have been identified at around 37 and 58 mbsf (Figure 4). The former spans about 12 cm (37.28–37.40 mbsf.) and is well
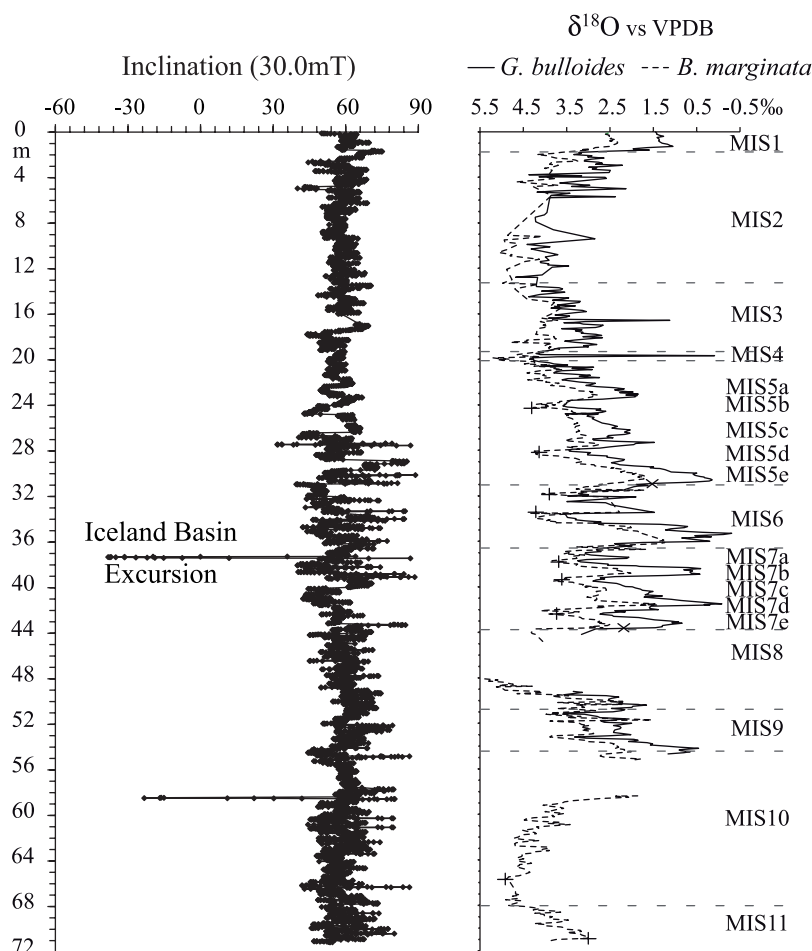
Figure 4. Geomagnetic inclination (°) for PRAD1-2 record. The oxygen stable isotope record shows the occurrence of the Iceland Basin geomagnetic Excursion (IBE) in correspondence to the boundary MIS 7/MIS 6.

defined in both magnetic declination and inclination. According to isotope stratigraphy, this excursion is close to the boundary between MIS 7 and MIS 6 and can be correlated with the Iceland Basin Excursion (IBE), occurring around 188 ka B.P. [*Laj et al.*, 2006] (Figure 4). Another reverse interval occurs at 58.45 mbsf, but it is characterized by only negative values of inclination that may reflect a strong overprint of the negative magnetization induced by the coring, rather than a true inversion. The position in which this potential geomagnetic excursion occurs in the borehole corresponds to the midpoint of the major oxygen stable isotopic shift of Termination IV, dated by *Lisiecki and Raymo* [2005], at 337 ka. Several authors report the presence of geomagnetic field excursions in the time interval between 315–340 ka B.P. [*Lund et al.*, 2006, and references therein]. If our interval with negative inclinations is representative of the geomagnetic field it could be associated with the CR1/9β excursion reported

by *Lund et al.* [2006] around 330 ka B.P. By integrating the dated excursion with the oxygen isotope curve, the Calabrian Ridge 1 (CR1) excursion as seen in core KC01-B appears to be younger than the deposition of Sapropel 10, i.e., located in an inconsistent position with respect to the excursion recognized in borehole PRAD1-2. Another possibility is that the potential excursion occurring at 58.45 mbsf in PRAD1-2 refers to the Agulhas Ridge-9β geomagnetic excursion that according to the review by *Oda* [2005] dated at about 335 ka B.P. and occurs close to the midpoint of Termination IV. However, because of the uncertainties discussed above this event was not included as control point in the proposed age-depth model of the borehole.

3.5. Radiometric Dating

[30] Calibrated ^{14}C ages (Table 1) chronologically constrain the following events:

[31] 1. The Last Glacial Maximum Chronozone, according to *Mix et al.* [2001], is defined between 19 and 23 cal. ka B.P. (i.e., 16.1–19.5 ^{14}C-ka B.P.). Interpolating the radiocarbon datings available in PRAD1-2, the LGM Chronozone is between 7.7 and 10.3 mbsf, positioned just above the interval of highest δ^{18}O values within MIS 2.

[32] 2. The Last Common Occurrence (LCO) of *G. inflata* during MIS 3 is identified at 16.9 mbsf in PRAD1-2. This event was identified in a coherent stratigraphic position in core RF93-77, collected in the same area [*Asioli*, 1996; *Trincardi et al.*, 1996, Figure 1], and shows a ^{14}C age of 39040 ± 800 years B.P. In core RF93-77, this bioevent slightly predates the Campanian Ignimbrite tephra [*Calanchi et al.*, 1998], corresponding to TM-18 of *Wulf et al.* [2004]. *Bourne* [2006] recognized the same tephra in 16.53–16.58 mbsf in PRAD1-2. Consequently, the consistent relative position of the Campanian Ignimbrite tephra and the LCO of *G. inflata* in both borehole PRAD1-2 and RF93-77 allow incorporating in the age-depth model the age determined on the latter core, after its recalibration according to *Fairbanks et al.* [2005].

[33] Two ages were obtained on *H. balthica* and *Elphidium crispum* from the same sample at 13.4 mbsf (Section 17 cm 60–62). The age provided by *H. balthica* is younger of 740 years ^{14}C age (780 calibrated years) than the one obtained on *E. crispum*. The preservation state is very good for both and reworking does not seem to explain the older age of *E. crispum*. Moreover, a selective bioturbation bringing specimens of *H. balthica* downward into older sediment does not seem very realistic. At present, the age obtained on *H. balthica* was preferred in the adopted age-depth model.

4. Sapropel Stratigraphy

[34] Sapropel layers have been defined on the basis of their content in organic matter (>2% according to the DSDP Leg 42A definition, 0.5–2% according to *Kidd et al.* [1978]). As summarized by *Cramp and O'Sullivan* [1999], these restrictive definitions have limited applicability because post depositional processes may significantly alter the amount of buried organic carbon. A less restrictive definition by *Hilgen* [1991], describing sapropels as "brownish, often laminated interbeds," is also difficult to apply because the lamination is not necessarily always present. PRAD1-2 lithology records dark and in some cases laminated sediment

layers accompanied by distinctive conditions in micropaleontological, geochemical and paleomagnetic parameters, all indicating fresh surface waters, accompanied by less-oxygenated seafloor conditions. Indeed, these intervals are characterized by extremely low values of δ^{18}O and δ^{13}C and minima in concentration-related magnetic parameters (e.g., ARM), lower color reflectance, and a characteristic foraminifera assemblage. Benthic foraminifera are generally present in all these events, except for two intervals (30.6–30.5 mbsf and 38.7–38.6 mbsf), where they are nearly absent (marked with a circle in the concentration curve in Figure 5). When present, benthic assemblage in correspondence to these levels is generally dominated by (deep-) infaunal taxa, such as *Uvigerina* spp, *Bolivina* + *Brizalina* (Figure 5) and *Fursenkoina* (*Globobulimina*, and *Chilostomella* are less frequent) as observed in deeper-water sapropels [*Jorissen*, 1999]. Seafloor oxygen deficiency is indicated by the Oxygen Deficiency Stress curve (ODS, Figure 5), which, according to *Rohling et al.* [1997], reflects severe low-oxygen stress before totally azoic conditions. Neogloboquadrinids (*Neogloboquadrina pachyderma* r.c. and *Neogloboquadrina dutertrei*) and/or *Globigerinoides ruber* (pink) dominate the Adriatic planktic assemblage during these events, consistently with reported planktic foraminiferal assemblages in the Mediterranean during the sapropel intervals [*Cita et al.*, 1977; *Rohling and Gieskes*, 1989; *Negri et al.*, 1999]. For these reasons we name these central Adriatic layers as sapropel equivalents (S1 equivalent, S3 equivalent and so on; Figure 5). Sapropel deposition is related to orbitally driven oscillations in the Northern Hemisphere insolation [*Rossignol-Strick*, 1983; *Hilgen*, 1991] and, in particular, records orbital precession minima and insolation maxima [*Lourens et al.*, 1996]. When recognized, visually or by means of geochemical/biological indicators, sapropels are therefore very useful to improve the chronology of sedimentary sequences.

[35] The ages ascribed to sapropel equivalents in PRAD1-2 refer to the sapropel-based astronomical timescale for the last 1.1 Ma established in the Ionian Sea, eastern Mediterranean [*Lourens*, 2004]. *Lourens* [2004] based the age calibration on sapropel midpoints (m), recognized visually or by geochemical changes for the "ghost" levels [*Langereis et al.*, 1997] and by the decrease in reflectance index and of the oxygen isotope shift to lower values. These ages are referred to their correlative insolation maxima, lagging 3 ka behind. Ascribing the ages to the sapropel equivalent layers
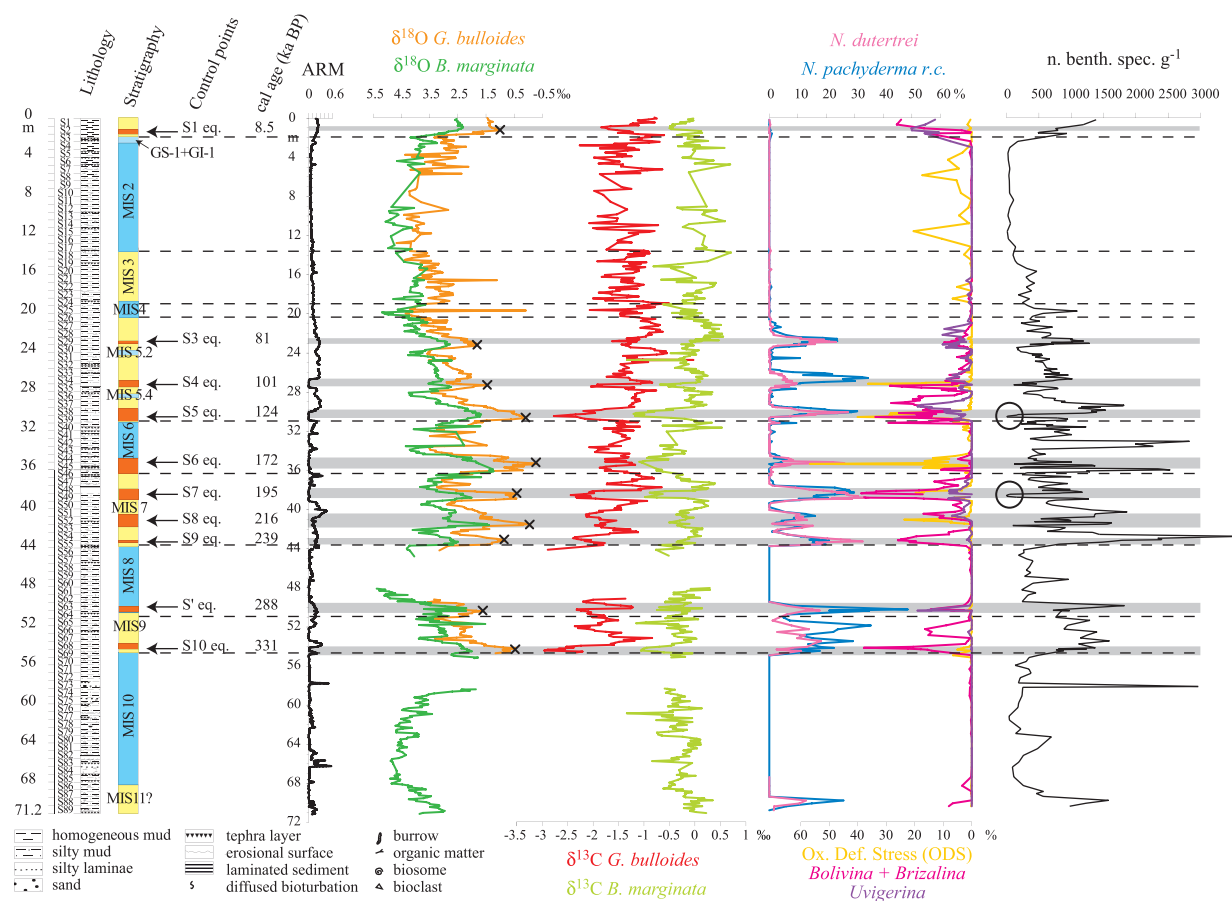
Figure 5. Most representative proxies that allow detection of sapropel equivalent beds in PRAD1-2. "X" symbols correspond to the control points with the lightest δ^{18}O values for each sapropel equivalent (according to *Lourens* [2004]). Oxygen Deficiency Stress (ODS) curve following the approach of *Rohling et al.* [1997]. Circles identify minima (quasi-absence) in benthic foraminifera concentration.

in PRAD1-2 core was based on the lowest δ^{18}O value present within each interval characterized by concurrent reflectance and ARM minima (Figures 5 and 6). This choice implies a synchronism between the δ^{18}O signal in the central Adriatic and the more oceanic Ionian Sea. The use of sapropel midpoints as age markers with a fixed time lag of 3 ka after the insolation peak is effective, but too coarse if applied to studies needing the exact timing of sapropels [*Emeis et al.*, 2003]. However, referring to the presently available literature, the problem of the exact timing of the upper Quaternary sapropels in the eastern Mediterranean seems to be difficult to solve, since only the age of Sapropel 1 can be assessed by calibrated radiocarbon dates [see, e.g., *Strohle and Krom*, 1997; *Mercone et al.*, 2000]. Alternatively, the base of each sapropel layer can be taken as reference level [*Emeis et al.*, 2003], imposing the synchronism with insolation maxima, or unambiguous bioevents, such as last or first zero abundance levels, along with O and C stable isotope

signals on shallow and deep-living species [*Cane et al.*, 2002; *Corselli et al.*, 2002; *Capotondi et al.*, 2006]. Even considering these problems, however, we maintain that the choice of the lowest δ^{18}O values as tie points is, at present, the most practical in assessing the chronological framework of the borehole. However, we are aware that in PRAD1-2 the onset or the demise of sapropel-equivalent beds may be slightly diachronous with respect to deeper water sapropels in the adjacent southern Adriatic or in the Mediterranean [cf. *Rohling*, 1999].

5. Dansgaard-Oeschger Events

[36] A fine-tuned correlation between PRAD1-2 and GISP2 δ^{18}O records is attempted for the last 80 ka. During this interval the isotopic record of GISP2 ice core [*Grootes et al.*, 1993; *Meese et al.*, 1997] reports several abrupt oscillations especially within the Last Glacial Period (MIS 4, MIS 3 and MIS 2), occurring with an average periodicity of
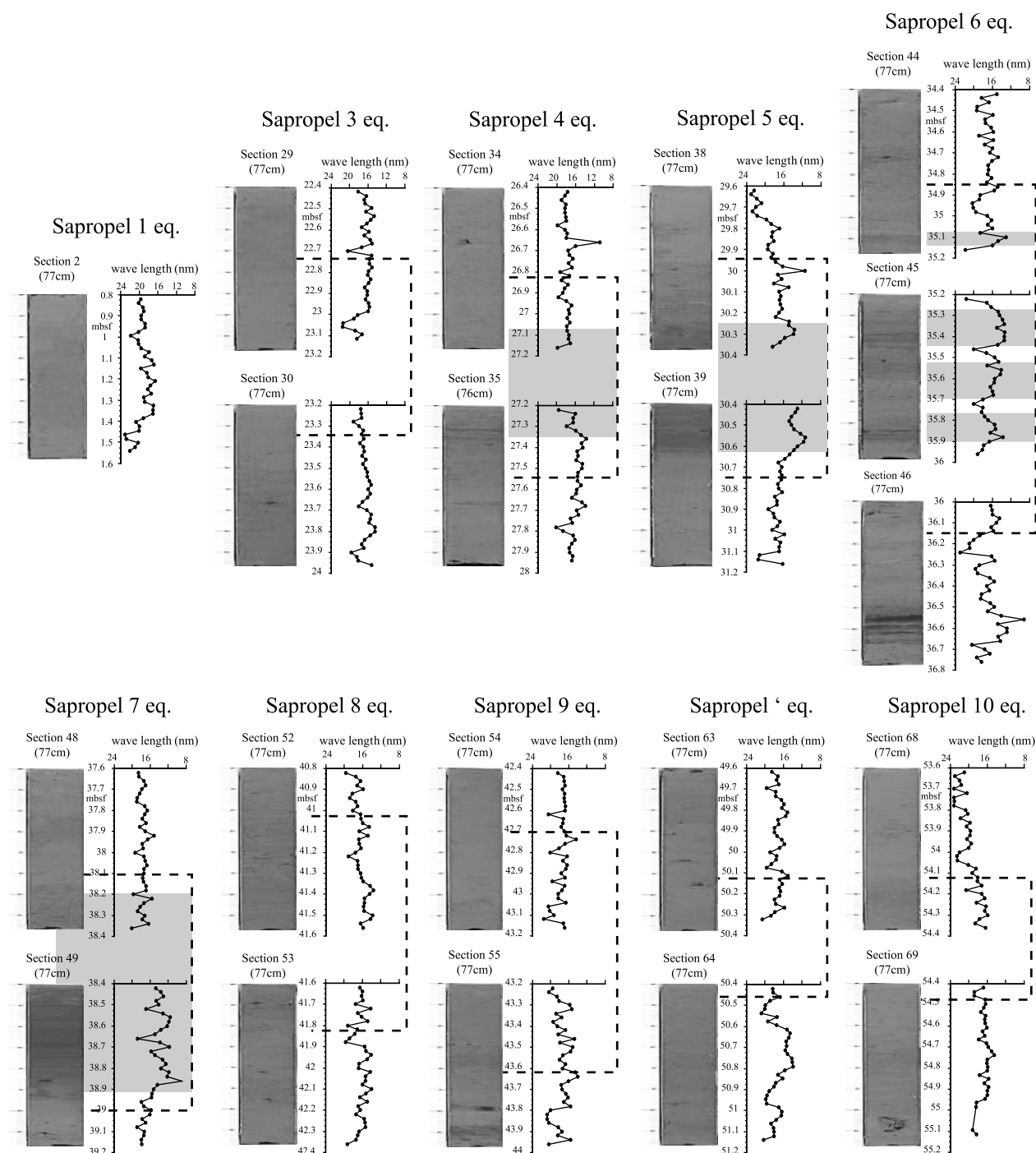
Figure 6. Visual (photographic) characterization of the main sapropel equivalent levels in PRAD1-2, along with the quantitative expression (by color reflectance values) of chromatic variations. Dashed lines identify the sapropelic anomaly; grey areas correspond to the darker color in the sediment.

1470 years [*Bond et al.*, 1997]. Abrupt subtle shifts toward lower $\delta^{18}O$ values, called Dansgaard-Oeschger events, were interpreted as short-lived, mild interstadials within the overall glacial interval [*Johnsen et al.*, 1972; *Dansgaard et al.*, 1982, 1993]. Clusters of Dansgaard-Oeschger events progressively decline in intensity and shift toward

higher isotope values, before culminating in the so-called Heinrich events. These intervals, well known in the North Atlantic, record drifting Arctic icebergs toward lower latitudes, which progressively melted, bringing colder and fresher water as well as spreading ice rafted detritus on the seafloor [*Clark*, 1994; *Baumann et al.*, 1995]. The group

of Dansgaard-Oeschger cycles between two Heinrich events consists of a Bond cycle [*Bond and Lotti*, 1995; *Bond et al.*, 1997, 1999]. These short-term oscillations, originally investigated in the North Atlantic (Iberian Margin in particular [e.g., *Lebreiro et al.*, 1996; *Schönfeld et al.*, 2003]), have been recognized in the western Mediterranean, including Alboran Sea and Gulf of Lions [e.g., *Rohling et al.*, 1998; *Cacho et al.*, 1999; *Combourieu Nebout et al.*, 2002; *Sanchez Goñi et al.*, 2002; *Martrat et al.*, 2004; *Sierro et al.*, 2005], and correlated even to eastern Mediterranean records [*Allen et al.*, 1999], implying a major atmospheric connection, involving a wider region of the Northern Hemisphere. These events were recognized worldwide on the basis of a variety of independent proxies [*Voelker and Workshop Participants*, 2002].

[37] The $\delta^{18}O$ curve obtained from the planktic *G. bulloides* in PRAD1-2 shows a higher resolution than the benthic one and is therefore used to compare to the $\delta^{18}O$ record of GISP2 (Figure 7). Wiggle matching of the two isotopic curves plotted versus time allows identification of the D-O events in PRAD1-2 during the last 80 ka (Figure 7). These oscillations typically display shifts from 0.1 to more than 1‰ (around 0.6‰ on average) that are higher than the analytical error (0.06‰). It is important to note that the time lag (~200 years) deriving from the visual wiggle match of GISP2 and PRAD1-2 records is generally within the standard deviation of the oldest ^{14}C AMS ages (400 years on average).

[38] Additional proxies, beside the PRAD1-2 $\delta^{18}O$ isotope curve, allow recognition of the most characteristic features of D-O events in the Adriatic. The Ca/Ti record, from XRF measurements, shows higher values matching each D-O event; indeed, this ratio, assumed as proxy of the carbonate content of the sediment, parallels rather consistently the oxygen isotope curve of the PRAD1-2 record (in agreement with other deeper-water records [e.g., *Hofmann et al.*, 2005]), but presents anomalous trends during glacial intervals. Around 29 ka, close to the MIS 3/MIS 2 boundary, the Ca/Ti ratio significantly increases, and the signal becomes less discernible along the entire MIS 2. A similar trend characterizes the upper part of MIS 4, as well. These observations reflect the combined biogenic and detrital source of Ca and suggest that a higher sediment supply of terrigenous carbonate by river runoff likely superimposed to D-O oscillations during glacial intervals,

where the local physiography of the area implies a closer location of the river mouths. However, even if the Ca/Ti ratio in the Adriatic basin reflects local changes in basin physiography and river regime, a relation to climatic changes can be recognized and compared to North Atlantic records.

[39] Also K/Ti ratio helps recognizing D-O events. K is dominantly present and gets concentrated in K-feldspar and illite. Ti is present in rutile (heavy mineral), can be subject to sorting and concentrates in the coarse fraction; this element is related to the sediment fraction preferentially brought by aeolian dust [*Lourens et al.*, 2001]. Variation in the K/Ti ratio in the PRAD1-2 record may be related to changes in the intensity of weathering and erosion but also to the location of the sediment source and to sediment transport processes. The imprint of D/O events on this ratio is most probably related to combined climate and sea level changes. Moreover, since tephra layers deposited in PRAD1-2 record are rich in K, a 5 points average smoothing was applied to K/Ti ratio curve, to reduce the noise.

[40] Sediment lightness also reports positive peaks, in good agreement with the suggested D-O oscillations. However, while every D-O event corresponds to a peak of lightness, not all positive peaks record a D-O event. The distribution of our foraminifera samples allows recognition of only the most intense D-O events, as peaks of warm-climate planktic species, consistently with the paleoclimate features described in literature.

[41] Matching the data set available by the proxies above mentioned, it has been possible to recognize most of the D-O stadial (S) and interstadial (IS) intervals, from S20 to IS3, on the basis of the identification of isotopic relative maxima and minima and to use them as control points, adopting the corresponding GISP2 ages [*Meese et al.*, 1997], to produce a more refined chronological framework for PRAD1-2 record in the top of the sequence. D-O events were chosen as control points only when an evident correspondence between the two isotopic records was found. The degree of resolution reached is so high that two ^{14}C AMS ages, occurring in a consistent position compared with D-O ages, but presenting a higher degree of uncertainty, because of their standard deviation, were not included in the age-depth model. The PRAD1-2 record provides the first identification of D-O events in a proximal shallow-marine setting, and contributes to confirm a super-regional climate

Table 2. Control Points Concurring in the Definition of the Age-Depth Model of Borehole PRAD1-2

mbsf	Event	Age, ka B.P.	Source
0	modern time	0	this study
0.6	LO *G. inflata*	6	*Ariztegui et al.* [2000]
1.288	S1	8.5	*Lourens* [2004]
1.8	top YD	12	*Asioli et al.* [1999]
5.976	^{14}C AMS	17.3	this study
7.8	^{14}C AMS	19.2	this study
13.4	^{14}C AMS	27.6	this study
13.8	D-O IS3	27.723	*Meese et al.* [1997]
14.0	D-O S4	28.287	*Meese et al.* [1997]
14.1	D-O IS4	28.941	*Meese et al.* [1997]
14.5	D-O S5	30.102	*Meese et al.* [1997]
14.6	D-O IS5	30.123	*Meese et al.* [1997]
14.8	D-O S6	32.913	*Meese et al.* [1997]
14.9	D-O IS6	33.455	*Meese et al.* [1997]
15.22	D-O S7	34.120	*Meese et al.* [1997]
15.3	D-O IS7	35.147	*Meese et al.* [1997]
15.5	D-O S8	35.706	*Meese et al.* [1997]
15.8	D-O IS8	38.201	*Meese et al.* [1997]
16.096	D-O S9	39.678	*Meese et al.* [1997]
16.386	D-O S11	41.497	*Meese et al.* [1997]
16.578	D-O IS11	42.486	*Meese et al.* [1997]
16.781	D-O S12	42.713	*Meese et al.* [1997]
16.9	^{14}C AMS (LCO *G. inflata* in MIS 3)	43.1	*Asioli* [1996]
17.3	D-O S13	46.194	*Meese et al.* [1997]
17.4	D-O IS13	46.911	*Meese et al.* [1997]
17.5	D-O S14	47.245	*Meese et al.* [1997]
18.4	D-O S16	54.331	*Meese et al.* [1997]
18.7	D-O IS16	56.238	*Meese et al.* [1997]
18.8	D-O S17	56.884	*Meese et al.* [1997]
18.9	D-O IS17	57.539	*Meese et al.* [1997]
19.486	D-O S18	60.524	*Meese et al.* [1997]
19.676	D-O IS18	61.870	*Meese et al.* [1997]
19.981	D-O S19a	64.441	*Meese et al.* [1997]
20.5	D-O IS19a	65.736	*Meese et al.* [1997]
20.6	D-O S19	66.022	*Meese et al.* [1997]
20.9	D-O IS19	68.437	*Meese et al.* [1997]
21.2	D-O S20	69.368	*Meese et al.* [1997]
21.6	D-O IS20	72.751	*Meese et al.* [1997]
21.8	D-O S21	73.623	*Meese et al.* [1997]
23.059	S3	81	*Lourens* [2004]
24.094	MIS 5.2	91	*Martinson et al.* [1987]
27.3	S4	101	*Lourens* [2004]
28	MIS 5.4	111	*Martinson et al.* [1987]
30.6	S5	124	*Lourens* [2004]
30.95	T II	130	*Lisiecki and Raymo* [2005]
32.5	MIS 6.2	135	*Martinson et al.* [1987]
33.581	MIS 6.4	152.5	*Martinson et al.* [1987]
35.3	S6	172	*Lourens* [2004]
37.32	IBE	188	*Laj et al.* [2006]
37.7	MIS 7.0	189.5	*Martinson et al.* [1987]
38.4	S7	195	*Lourens* [2004]
39.5	MIS 7.2	200.5	*Martinson et al.* [1987]
41.5	S8	216	*Lourens* [2004]
42.4	MIS 7.4	225	*Martinson et al.* [1987]
43.2	S9	239	*Lourens* [2004]
43.65	T III	243	*Lisiecki and Raymo* [2005]
49.551	FO *E. huxleyi*	264	*Lourens* [2004]
50.4	S'	288	*Lourens* [2004]

Table 2. (continued)

mbsf	Event	Age, ka B.P.	Source
54.2	S10	331	*Lourens* [2004]
65.696	MIS 10.2?	340	*Bassinot et al.* [1994]
70.8	MIS 11.1?	364	*Bassinot et al.* [1994]

linkage impacting beyond the northern Atlantic, and extending to the entire Mediterranean.

6. Age Model

[42] The integrated stratigraphy discussed above is summarized in Figure 8 and adopted to propose a refined age-depth model for PRAD1-2 borehole (Figure 9) based on the control points reported on Table 2. This age model derives from a combination of control points that includes the midpoints of the isotopic Terminations (II and III), the isotopic correlation with other records in regard with substages maxima or minima, major and well known biostratigraphic events (LO or LCO, both based on foraminifera and nannoplankton), on available ^{14}C AMS calibrated ages, and on the recognition of a well dated polarity inversion of the magnetic field (IBE). Moreover, the identification of sapropel-like and D-O type events within the Last Glaciation (MIS 4-MIS 2), respectively, concur in strengthening the proposed age model.

[43] In summary, this age model shows maximum accumulation rates on the upper slope during glacial intervals MIS 10 and MIS 2 (Figure 9), while MIS 8 and MIS 6 show intermediate rates. The very high sedimentation rate during MIS 10 reflects the proximal location of the site during that interval. In contrast, the considerable increase in sediment accumulation rates (Figure 9) during MIS 2, starting circa 25 ka B.P., is marked by an abrupt shift in the Ca/Ti curve (Figure 7), suggesting an enhanced influence from the Alpine sources feeding the Po low stand delta, at that time located just few tens of km north of borehole PRAD1-2. The reader is referred to Ridente et al. (submitted manuscript, 2007) for a detailed discussion on PRAD1-2 accumulation rates.

7. Refined Bioevent Ages

[44] The age-depth model produced for PRAD1-2 allows an improved calibration of the age of the

Table 3. Calculated Calibrated Ages of the Main New Bioevents in PRAD1-2[a]

Depth in Core, mbsf	Event	Stratigraphic Position	PRAD1-2 Age, ka B.P.	Literature Age, ka B.P.
12	Entry of *S. sellii*	MIS 2 (between DOIS 3 and base LGM chronozone)	25.5	15.3 ka B.P. (^{14}C age from *Jorissen et al.* [1993])
14	LCO of *H. balthica*	DOIS 3–4 (approximates MIS 3/2 boundary)	28.3	
16.9	LCO of *G. inflata* in MIS3	MIS 3 (DOIS 12)	43.1	
30.6	Entry of *H. balthica*	Base MIS 5 (during S5 equiv.)	124	
31.2	LO *I. islandica*	MIS 6-MIS 5 boundary	131	
34.4	LO *E. excavatum* f. *clavata*	MIS 6.5–6.4 boundary	162	MIS 6 [*Borsetti et al.*, 1995]

[a] The stratigraphic position is reported as well as the corresponding ages in literature. DOS, Dansgaard-Oeschger Stadials; DOIS, Dansgaard-Oeschger Interstadials.
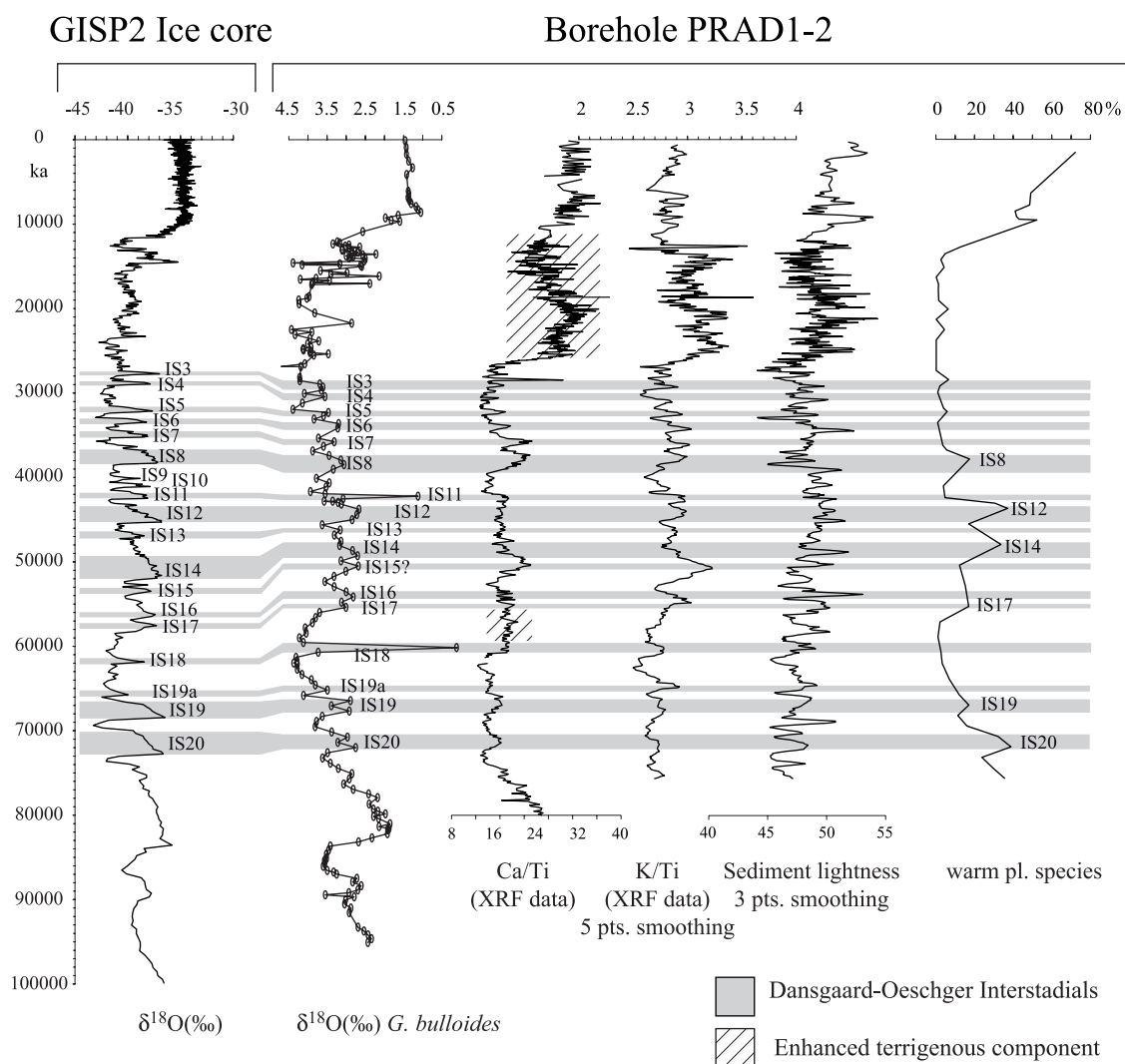

Figure 7. Dansgaard-Oeschger Interstadials (IS), highlighted in grey, in PRAD1-2 record after its correlation with GISP2 ice core.
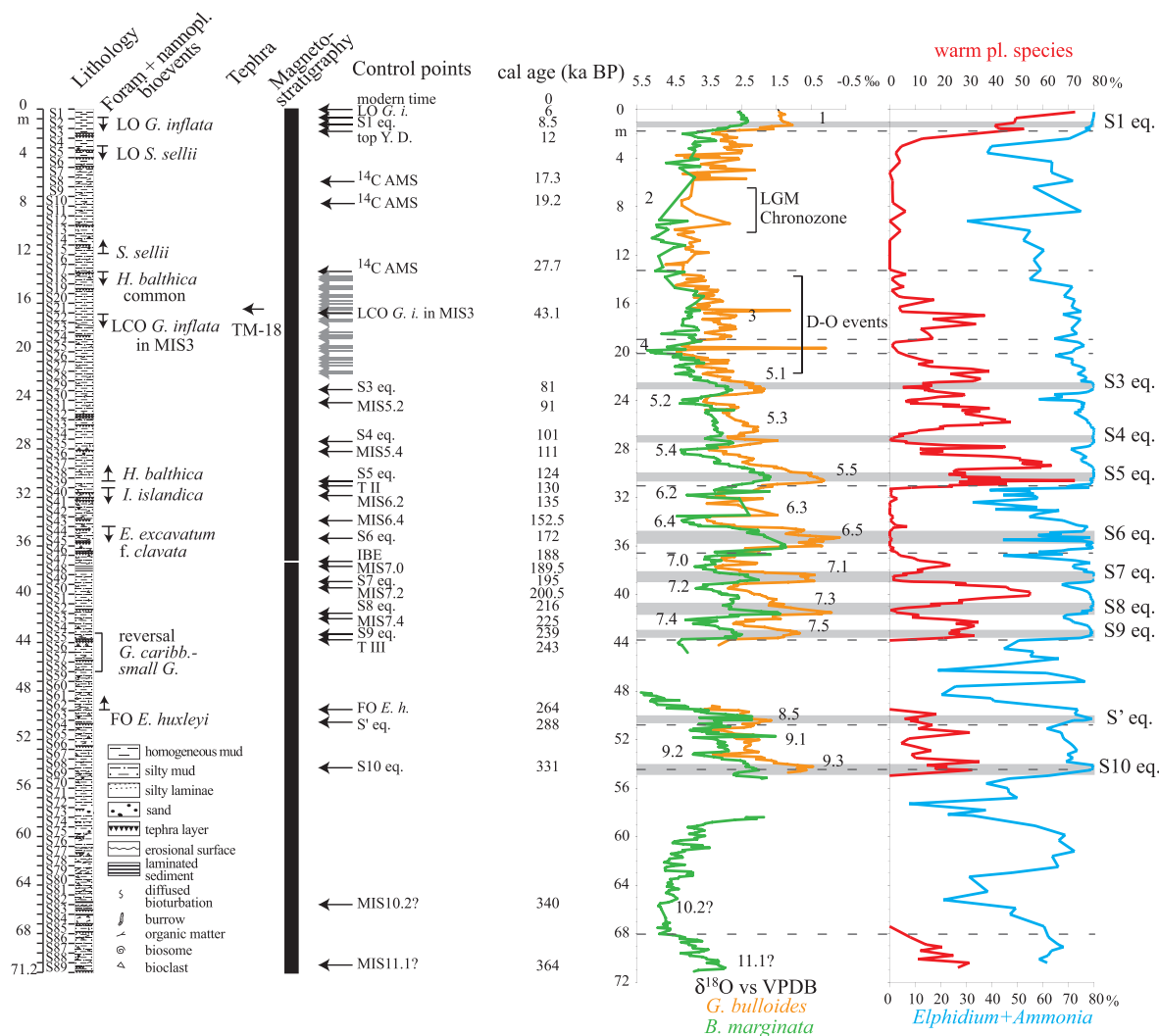
Figure 8. PRAD1-2 stratigraphic framework based on a multiproxy approach. Grey arrows correspond to the control points of Dansgaard-Oeschger events.

bioevents detected in the borehole. Table 3 summarizes these events along with their stratigraphic position. Some age discrepancies are present: For instance, the age of the entry of *S. sellii* is quite older than the age calculated by *Jorissen et al.* [1993] for the southern Adriatic.

8. Conclusion

[45] The proposed high-resolution stratigraphy for borehole PRAD1-2 is based on a multiproxy approach, including isotope stratigraphy, foraminifera and nannoplankton bioevents, foraminifera warm-cold cyclicity, magnetostratigraphy, ^{14}C AMS radiometric ages and the recognition, for the first time in the shallow-water central Adriatic, of ten sapropel equivalent layers (through correlation with a time-equivalent and orbitally-tuned record

available in the Ionian Sea) and of several stadial and interstadial D-O events, correlated with GISP2 ice core record. These integrated and independent proxies allow ascribing the borehole record to the time-interval from late MIS 11 to the Holocene. PRAD1-2 is therefore the most expanded and continuous marine record available for the Adriatic Basin, in which Milankovitch cyclicities can be recognized including the 100 ka (eccentricity-related glacial-interglacial oscillations) and the 23 ka (precession-related recurrence of sapropel deposits). In addition, the wiggle-match correlation between GISP2 ice core and PRAD1-2 records within the last glaciation (latest MIS 5–MIS 2) shows that a higher stratigraphic resolution can be achieved by recognizing Dansgaard-Oeschger events. These events provide additional control points and lead to a more refined age-depth model
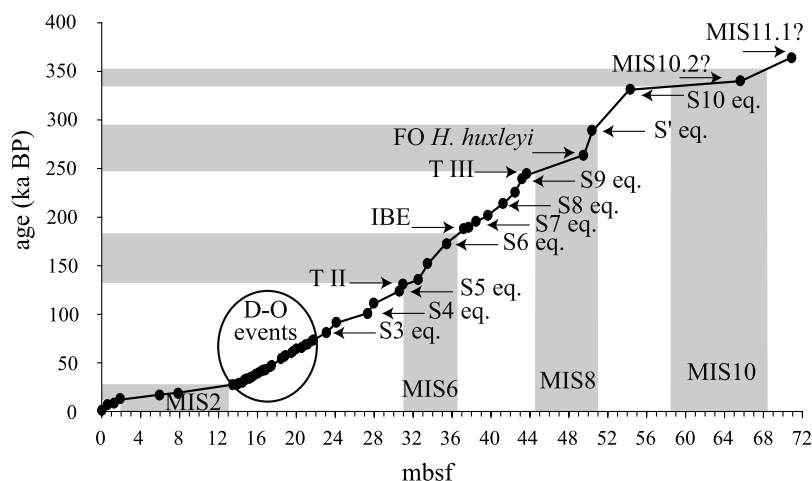
Figure 9. Age-depth model calculated for borehole PRAD1-2. Grey areas correspond to glacial intervals. The identified sapropel equivalent events allow refining the model by including the midpoint ages from *Lourens* [2004]. The age model in the upper portion of the borehole is further refined by the identification of the Dansgaard-Oeschger events (marked as D-O). See text for explanation.

for the upper portion of PRAD1-2. Despite the limited water-depth of the site (186 m), PRAD1-2 record is only slightly affected by local distortions induced by the land-locked position of the Adriatic Sea and presents clear evidence of linkages with both the eastern Mediterranean (sapropels) and the North Atlantic (D-O events) paleoclimatic histories. These linkages confirm the potential of this area to be correlated with more oceanic records, worldwide. The proposed age model can be refined by studying the numerous tephra layers recognized in PRAD1-2. This study will in turn allow testing possible leads or lags in the timing of key events like sapropels and D-O events at Mediterranean or hemispheric scale. Finally, the high accumulation rates of PRAD1-2 record have the potential of achieving centennial or decadal scale reconstructions and will help to better understand the timing (synchronism) between the events recognized in the Adriatic Sea and global climate changes.

Acknowledgments

References

Allen, J. R. M., et al. (1999), Rapid environmental changes in southern Europe during the last glacial period, *Nature*, *400*, 740–743.

Amorosi, A., M. L. Colalongo, F. Fusco, G. Pasini, and F. Fiorini (1999), Glacio-eustatic control of continental-shallow marine cyclicity from Late Quaternary deposits of the southeastern Po plain, northern Italy, *Quat. Res.*, *52*, 1–13.

Amorosi, A., M. L. Colalongo, F. Fiorini, F. Fusco, G. Pasini, S. C. Vaiani, and G. Sarti (2004), Palaeogeographic and palaeoclimatic evolution of the Po Plain from 150-ky core records, *Global Planet. Change*, *40*, 55–78.

Ariztegui, D., et al. (2000), Palaeoclimatic reconstructions and formation of sapropel S1: Inferences from Late Quaternary lacustrine and marine sequences in the Central Mediterranean region, *Palaeogeogr. Palaeoclimatol. Palaeoecol.*, *158*(3/4), 215–240.

Asioli, A., (1996), High resolution foraminifera biostratigraphy in the central Adriatic basin during the last deglaciation: A contribution to the PALICLAS Project, in *Palaeoenvironmental Analysis of Italian Crater Lake and Adriatic Sediments*, *Mem. Ist. Ital. Idrobiol.*, vol. 55, edited by F. Oldfield and P. Guilizzoni, pp. 197–218, Ist. Ital. di Idrobiol., Verbania-Pallanza, Italy.

Asioli, A., F. Trincardi, J. J. Lowe, and F. Oldfield (1999), Short-term climate changes during the Last Glacial-Holocene transition: Comparison between Mediterranean records and the GRIP event stratigraphy, *J. Quat. Sci.*, *14*, 373–381.

Asioli, A., F. Trincardi, J. J. Lowe, D. Ariztegui, L. Langone, and F. Oldfield (2001), Sub-millennial scale climatic oscillations in the central Adriatic during the Lateglacial: Palaeoceanographic implications, *Quat. Sci. Rev.*, *20*, 1201–1221.

Bassinot, F. C., L. D. Labeyrie, E. Vincent, X. Quidelleur, N. J. Shackleton, and Y. Lancelot (1994), The astronomical theory of climate and the age of the Brunhes Matuyama magnetic reversal, *Earth Planet. Sci. Lett.*, *126*, 91–108.

Baumann, K.-H., K. S. Lackschewitz, J. Mangerud, R. F. Spielhagen, T. C.W. Wolf-Welling, R. Heinrich, and

H. Kassens (1995), Reflection of Scandinavian Ice Sheet fluctuations in Norwegian Sea sediments during the last 150,000 years, *Quat. Res.*, *43*, 185–197.

Bond, G., and R. Lotti (1995), Iceberg discharge into the North Atlantic on millennial time scales during the Last Glaciation, *Science*, *267*, 1005–1010.

Bond, G., W. Showers, M. Cheseby, R. Lotti, P. Almasi, P. deMenocal, P. Priore, H. Cullen, I. Hajdas, and G. Bonani (1997), A pervasive millennial-scale cycle in North Atlantic Holocene and glacial climates, *Science*, *278*, 1257–1266.

Bond, G. B., W. Showers, M. Elliot, et al. (1999), The North Atlantic's 1–2 kyr climate rhythm: Relation to Heinrich events, Dansgaard-Oeschger cycles and the Little Ice Age, in *Mechanisms of Global Climate Change at Millennial Time Scales*, *Geophys. Monogr. Ser.*, vol. 112, edited by P. U. Clark, R. S. Webb, and L. D. Keigwin, pp. 35–58, AGU, Washington, D. C.

Borsetti, A. M., L. Capotondi, F. Cati, A. Negri, C. Vergnaud-Grazzini, C. Alberini, P. Colantoni, and P. Curzi (1995), Biostratigraphic events and Late Quaternary tectonics in the Dosso Gallignani (central-southern Adriatic Sea), *G. Geol.*, *57*(1–2), 41–58.

Bourne, A. J. (2006), An initial tephrochronology for the Adriatic core PRAD1-2 for 40 ka BP, M.Sc. thesis, 172 pp., Royal Holloway, Univ. of London, London.

Butzin, M., M. Prange, and G. Lohmann (2005), Radiocarbon simulations for the glacial ocean: The effects of wind stress, Southern Ocean sea ice and Heinrich events, *Earth Planet. Sci. Lett.*, *235*, 45–61.

Cacho, I., J. O. Grimalt, C. Pelejero, M. Canals, F. J. Sierro, J. A. Flores, and N. J. Shackleton (1999), Dansgaard-Oeschger and Heinrich event imprints in Alboran Sea paleotemperatures, *Paleoceanography*, *14*(6), 698–705.

Calanchi, N., A. Cattaneo, E. Dinelli, G. Gasparotto, and F. Lucchini (1998), Tephra layers in Late Quaternary sediments of the central Adriatic Sea, *Mar. Geol.*, *149*, 191–209.

Cane, T., E. J. Rohling, A. E.S. Kemp, S. Cooke, and R. B. Pearce (2002), High-resolution stratigraphic framework for Mediterranean sapropel S5: Defining temporal relationships between records of Eemian climate variability, *Palaeogeogr. Palaeoclimatol. Palaeoecol.*, *183*, 87–101.

Capotondi, L., M. S. Principato, C. Morigi, F. Sangiorgi, P. Maffioli, S. Giunta, A. Negri, and C. Corselli (2006), Foraminiferal variations and stratigraphic implications to the deposition of sapropel S5 in the eastern Mediterranean, *Palaeogeogr. Palaeoclimatol. Palaeoecol.*, *235*, 48–65.

Cattaneo, A., and F. Trincardi (1999), The late-Quaternary transgressive record in the Adriatic epicontinental sea: Basin widening and facies partitioning, in *Isolated Shallow Marine Sand Bodies: Sequence Stratigraphic Analysis and Sedimentologic Interpretation*, edited by K. Bergman and J. Snedden, *Spec. Publ. SEPM Soc. Sediment. Geol.*, *64*, 127–146.

Cita, M. B., C. Vergnaud Grazzini, C. Robert, H. Chamley, N. Ciaranfi, and S. D'Onofrio (1977), Paleoclimatic record of a long deep sea core from the eastern Mediterranean, *Quat. Res.*, *8*, 205–235.

Clark, P. U. (1994), Unstable behaviour of the Laurentide Ice Sheet over deforming sediment and its implications for climate change, *Quat. Res.*, *41*, 19–25.

Colmenero-Hidalgo, E., J. A. Flores, and F. J. Sierro (2002), Biometry of Emiliania huxleyi and its biostratigraphic significance in the eastern north Atlantic Ocean and western Mediterranean Sea in the last 20,000 years, *Mar. Micropaleontol.*, *46*, 247–263.

Combourieu Nebout, N., J. L. Turon, R. Zahn, L. Capotondi, L. Londeix, and K. Pahnke (2002), Enhanced aridity and atmospheric high-pressure stability over the western Mediterranean during the North Atlantic cold events of the past 50 k.y., *Geology*, *30*(10), 863–866.

Corselli, C., M. S. Principato, P. Maffioli, and D. Crudeli (2002), Changes in planktonic assemblages during sapropel S5 deposition: Evidence from Urania Basin area, eastern Mediterranean, *Paleoceanography*, *17*(3), 1029, doi:10.1029/2000PA000536.

Cramp, A., and G. O'Sullivan (1999), Neogene sapropels in the Mediterranean: A review, *Mar. Geol.*, *153*, 11–28.

Croudace, I. W., R. Anders, and R. G. Rothwell (2006), ITRAX: Description and evaluation of a new multi-function X-ray core scanner, in *New Techniques in Sediment Core Analysis*, edited by R. G. Rothwell, *Spec. Publ. Geol. Soc.*, *267*, 51–63.

Dansgaard, W., H. B. Clausen, N. Gundestrup, C. U. Hammer, S. J. Johnsen, P. M. Kristindottir, and N. Reeh (1982), A new Greenland deep ice core, *Science*, *218*, 1273–1277.

Dansgaard, W., et al. (1993), Evidence for general instability of past climate from a 250-kyr ice-core record, *Nature*, *364*, 218–220.

de Stigter, H. C., F. J. Jorissen, and G. J. van der Zwaan (1998), Bathymetric distribution and microhabitat partitioning of live (Rose Bengal stained) benthic foraminifera along a shelf to bathyal transect in the southern Adriatic Sea, *J. Foraminiferal Res.*, *28*, 40–65.

Emeis, K.-C., et al. (2003), Eastern Mediterranean surface water temperatures and $\delta^{18}O$ composition during deposition of sapropels in the late Quaternary, *Paleoceanography*, *18*(1), 1005, doi:10.1029/2000PA000617.

Fairbanks, R. G., R. A. Mortlock, T.-C. Chiu, L. Cao, A. Kaplan, T. P. Guilderson, T. W. Fairbanks, and A. L. Bloom (2005), Marine radiocarbon calibration curve spanning 0 to 50,000 years B. P. based on paired $^{230}Th/^{234}U/^{238}U$ and ^{14}C dates on pristine corals, *Quat. Sci. Rev.*, *24*, 1781–1796.

Flores, J.-A., R. Gersonde, and F. J. Sierro (1999), Pleistocene fluctuations in the Agulhas current retroflections based on the calcareous plankton record, *Mar. Micropaleontol.*, *37*, 1–22.

Grootes, P. M., M. Stuiver, J. W.C. White, S. Johnsen, and J. Jouzel (1993), Comparison of oxygen isotope records from the GISP2 and GRIP Greenland ice cores, *Nature*, *366*, 552–554.

Guilizzoni, P., and F. Oldfield (Eds.) (1996), *Palaeoenvironmental Analysis of Italian Crater Lake and Adriatic Sediments*, *Mem. Ist. Ital. Idrobiol.*, vol. 55, Ist. Ital. di Idrobiol., Verbania-Pallanza, Italy.

Hemleben, C., M. Spindler, and O. R. Anderson (Eds.) (1989), *Modern Planktic Foraminifera*, Springer, New York.

Hilgen, F. J. (1991), Astronomical calibration of Gauss to Matuyama sapropels in the Mediterranean and implication for the geomagnetic polarity time scale, *Earth Planet. Sci. Lett.*, *104*, 226–244.

Hine, N., and P. P. E. Weaver (1998), Quaternary, in *Calcareous Nannofossil Biostratigraphy*, edited by P. R. Bown, pp. 266–283, Chapman and Hall, London.

Hofmann, D. I., K. Fabian, F. Schmieder, B. Donner, and U. Bleil (2005), A stratigraphic network across the Subtropical Front in the central South Atlantic: Multi-parameter correlation of magnetic susceptibility, density, X-ray fluorescence and $\delta^{18}O$ records, *Earth Planet. Sci. Lett.*, *240*, 694–709.

Hughen, K. A., et al. (2004), Marine04 marine radiocarbon age calibration, 0–26 Cal kyr BP, *Radiocarbon*, *46*(3), 1059–1086.

Jansen, J. H. F., S. J. Van der Gaast, B. Koster, and A. J. Vaars (1998), CORTEX, a shipboard XRF-scanner for element analyses in split sediment cores, *Mar. Geol.*, *151*(1−4), 143−153.

Johnsen, S. J., W. Dansgaard, H. B. Clausen, and C. C. Langway Jr. (1972), Oxygen isotope profiles through the Antarctic and Greenland ice sheets, *Nature*, *359*, 311−313.

Jorissen, F. J. (1987), The distribution of benthic foraminifera in the Adriatic Sea, *Mar. Micropaleontol.*, *12*, 21−48.

Jorissen, F. J. (1988), Benthic foraminifera from the Adriatic Sea: Principles of phenotypic variation, *Utrecht Micropaleontol. Bull.*, *37*, 174 pp.

Jorissen, F. J. (1999), Benthic foraminiferal successions across Late Quaternary Mediterranean sapropels, *Mar. Geol.*, *153*, 91−101.

Jorissen, F. J., A. Asioli, A. M. Borsetti, L. Capotondi, J. P. De Visser, F. J. Hilgen, E. J. Rohling, K. Van Der Borg, C. Vergnaud-Grazzini, and W. J. Zachariasse (1993), Late Quaternary central Mediterranean biochronology, *Mar. Micropaleontol.*, *21*, 169−189.

Kidd, R. B., M. B. Cita, and W. B.F. Ryan (1978), Stratigraphy of eastern Mediterranean sapropel sequences recovered during Leg 42A and their paleoenvironmental significance, *Initial Rep. Deep Sea Drill. Proj.*, *42A*, 421−443.

Laj, C., C. Kissel, and A. P. Roberts (2006), Geomagnetic field behavior during the Iceland Basin and Laschamp geomagnetic excursions: A simple transitional field geometry?, *Geochem. Geophys. Geosyst.*, *7*, Q03004, doi:10.1029/2005GC001122.

Langereis, C. G., M. J. Dekkers, G. J. De Lange, M. Paterne, and P. J. M. Van Santvoort (1997), Magnetostratigraphy and astronomical calibration of the last 1.1 Myr from an eastern Mediterranean piston core and dating of short events in the Brunhes, *Geophys. J. Int.*, *129*, 75−94.

Lebreiro, S. M., J. C. Moreno, I. N. McCave, and P. P. E. Weaver (1996), Evidence for Heinrich layers off Portugal (Tore Seamount: 39°N, 12°W), *Mar. Geol.*, *131*, 47−56.

Lisiecki, L. E., and M. E. Raymo (2005), A Pliocene-Pleistocene stack of 57 globally distributed benthic δ^{18}O records, *Paleoceanography*, *20*, PA1003, doi:10.1029/2004PA001071.

Lourens, L. J. (2004), Revised tuning of Ocean Drilling Program Site 964 and KC01B (Mediterranean) and implications for the δ^{18}O, tephra, calcareous nannofossil, and geomagnetic reversal chronologies of the past 1.1 Myr, *Paleoceanography*, *19*, PA3010, doi:10.1029/2003PA000997.

Lourens, L. J., A. Antonarakou, F. J. Hilgen, A. A. M. Van Hoof, C. Vergnaud-Grazzini, and W. J. Zachariasse (1996), Evaluation of the Plio-Pleistocene astronomical timescale, *Paleoceanography*, *11*, 391−413.

Lourens, L. J., R. Wehausen, and H. J. Brumsack (2001), Geological constraints on tidal dissipation and dynamical ellipticity of the Earth over the past three million years, *Nature*, *409*(6823), 1029−1033.

Lund, S., J. S. Stoner, J. E. T. Channel, and G. Acton (2006), A summary of Brunhes paleomagnetic field variability recorded in the Ocean Drilling Program cores, *Phys. Earth Planet. Inter.*, *156*, 194−204.

Martini, E. (1971), Standard Tertiary and Quaternary calcareous nannoplankton zonation, in *Proceedings 2nd International Conference on Planktonic Microfossils Roma*, vol. 2, edited by A. Farinacci, pp. 739−785, Tecnoscience, Rome.

Martinson, D. G., N. G. Pisias, J. D. Hays, J. Imbrie, T. C. Moore, and N. J. Shackleton (1987), Age dating and the orbital theory of the ice ages: development of a high-resolution 0 to 300,000-year chronostratigraphy, *Quat. Res.*, *27*, 1−29.

Martrat, B., J. O. Grimalt, C. Lopez-Martinez, I. Cacho, F. J. Sierro, J. A. Flores, R. Zahn, M. Canals, J. H. Curtis, and D. A. Hodell (2004), Abrupt temperature changes in the western Mediterranean over the past 250,000 years, *Science*, *306*, 1762−1765.

Massari, F., D. Rio, R. Serandrei Barbero, A. Asioli, L. Capraro, E. Fornaciari, and P. P. Vergerio (2004), The environment of Venice area in the past two million years, *Palaeogeogr. Palaeoclimatol. Palaeoecol.*, *202*, 273−308.

Meese, D. A., A. J. Gow, R. B. Alley, G. A. Zielinsky, P. M. Grootes, M. Ram, K. C. Taylor, P. A. Mayewski, and J. F. Bolzan (1997), The Greenland Ice Sheet Project 2 depth-age scale: Methods and results, *J. Geophys. Res.*, *102*(12), 26,411−26,423.

Mercone, D., J. Thomson, I. W. Croudace, G. Siani, M. Paterne, and S. Troelstra (2000), Duration of S1, the most recent sapropel in the eastern Mediterranean Sea, as indicated by accelerator mass spectrometry radiocarbon and geochemical evidence, *Paleoceanography*, *15*, 336−347.

Mix, A. C., E. Bard, and R. Schneider (2001), Environmental processes of the ice age: Land, oceans, glaciers (EPILOG), *Quat. Sci. Rev.*, *20*, 627−657.

Murray, J. W. (2006), *Ecology and Applications of Benthic Foraminifera*, Cambridge Univ. Press, New York.

Negri, A., L. Capotondi, and J. Keller (1999), Calcareous nannofossils, planktonic foraminifera and oxygen isotopes in the late Quaternary sapropels of the Ionian Sea, *Mar. Geol.*, *157*, 89−103.

Oda, H. (2005), Recurrent geomagnetic excursions: A review for the Brunhes normal polarity chron, *J. Geogr.*, *114*(2), 174−193.

Piva, A., A. Asioli, N. Andersen, J. O. Grimalt, R. R. Schneider, and F. Trincardi (2008), Climatic cycles as expressed in sediments of the PROMESS1 borehole PRAD1-2, central Adriatic, for the last 370 ka: 2. Paleoenvironmental evolution, *Geochem. Geophys. Geosyst.*, doi:10.1029/2007GC001785, in press.

Pujol, C., and C. Vergnaud Grazzini (1995), Distribution patterns of live planktic foraminifera as related to regional hydrography and productive systems of the Mediterranean sea, *Mar. Micropaleontol.*, *25*, 187−217.

Richter, T. O., S. Van Der Gaast, R. Koster, A. Vaars, R. Gieles, H. C. de Stigter, H. de Haas, and T. C. E. van Weering (2006), The AVAATECH XRF Core Scanner: Technical description and applications to NE Atlantic sediments, in *New Techniques in Sediment Core Analysis*, edited by R. G. Rothwell, *Spec. Publ. Geol. Soc.*, *267*, 39−50.

Rio, D., I. Raffi, and G. Villa (1990), Pliocene-Pleistocene calcareous nannofossil distribution patterns in the western Mediterranean, *Proc. Ocean Drill. Program Sci. Results*, *107*, 513−533.

Rohling, E. J. (1999), Environmental controls on salinity and δ^{18}O in the Mediterranean, *Paleoceanography*, *14*, 706−715.

Rohling, E. J., and W. W. C. Gieskes (1989), Late Quaternary changes in Mediterranean intermediate water density and formation rate, *Paleoceanography*, *4*, 531−545.

Rohling, E. J., F. J. Jorissen, and H. C. de Stigter (1997), 200 year interruption of Holocene sapropel formation in the Adriatic Sea, *J. Micropaleontol.*, *16*, 97−108.

Rohling, E. J., A. Hayes, S. De Rijk, D. Kroon, W. J. Zachariasse, and D. Eisma (1998), Abrupt cold spells in the northwestern Mediterranean, *Paleoceanography*, *13*(4), 316−322.

Rossignol-Strick, M. (1983), African monsoons, an immediate climate response to orbital insolation, *Nature*, *304*, 46–49.

Sanchez Goñi, M. F., I. Cacho, J. L. Turon, J. Guiot, F. J. Sierro, J. P. Peypouquet, J. O. Grimalt, and N. J. Shackleton (2002), Synchroneity between marine and terrestrial responses to millennial scale climatic variability during the last glacial period in the Mediterranean region, *Clim. Dyn.*, *19*, 95–105.

Schönfeld, J., R. Zahn, and L. de Abreu (2003), Surface and deep water response to rapid climate changes at the Western Iberian Margin, *Global Planet. Change*, *36*, 237–264.

Sen Gupta, B. K. (1999), *Modern Foraminifera*, Kluwer Acad., Norwell, Mass.

Sierro, F. J., et al. (2005), Impact of iceberg melting on Mediterranean thermohaline circulation during Heinrich events, *Paleoceanography*, *20*, PA2019, doi:10.1029/2004PA001051.

Skene, K., D. Piper, A. Aksu, and J. P. M. Syvitski (1998), Evaluation of the global oxygen isotope curve as a proxy for quaternary sea-level by modeling of delta progradation, *J. Sediment. Res.*, *68*(6), 1077–1092.

Strohle, K., and M. D. Krom (1997), Evidence for the evolution of an oxygen minimum layer at the beginning of S-1 sapropel deposition in the eastern Mediterranean, *Mar. Geol.*, *140*, 231–236.

Stuiver, M., and T. F. Braziunas (1993), ^{14}C ages of marine samples to 10,000 BC, *Radiocarbon*, *35*(1), 137–189.

Stuiver, M., and P. J. Reimer (1993), Extended ^{14}C data base and revised CALIB 3.0 ^{14}C age calibration program, *Radiocarbon*, *35*, 215–230.

Sydow, J., and H. H. Roberts (1994), Stratigraphic framework of late Pleistocene shelf edge delta, northeast Gulf of Mexico, *AAPG Bull.*, *78*(8), 1276–1312.

Thierstein, H. R., K. Geitzenauer, B. Molfino, and N. J. Shackleton (1977), Global synchronicity of late Quaternary coccolith datum levels: validation by oxygen isotopes, *Geology*, *5*, 400–404.

Trincardi, F., A. Cattaneo, A. Asioli, A. Correggiari and L. Langone (1996), Stratigraphy of the late-Quaternary deposits in the central Adriatic basin and the record of short-term climatic events, in *Palaeoenvironmental Analysis of Italian Crater Lake and Adriatic Sediments*, *Mem. Ist. Ital. Idrobiol.*, vol. 55, edited by F. Oldfield and P. Guilizzoni, pp. 39–70, Ist. Ital. di Idrobiol., Verbania-Pallanza, Italy.

Van der Zwaan, G. J., and F. J. Jorissen (2002), Biofacial patterns in river-induced anoxia, in *Modern and Ancient Continental Shelf Anoxia*, edited by R. Tyson and T. H. Pearson, *Spec. Publ. Geol. Soc.*, *58*, 65–82.

Villanueva, J., J.-A. Flores, and J. O. Grimalt (2002), A detailed comparison of the $U_{37}^{k'}$ and coccolith records over the past 290 kyears: Implications to the alkenone paleotemperature method, *Org. Geochem.*, *33*, 897–905.

Voelker, A. H. L., and Workshop Participants (2002), Global distribution of centennial-scale records for Marine Isotope Stage (MIS) 3: A database, *Quat. Sci. Rev.*, *21*, 1185–1212.

Wulf, S., M. Kraml, A. Brauer, J. Keller, and J. F. W. Negendank (2004), Tephrochronology of the 100 ka lacustrine sediment record of Lago Grande di Monticchio (southern Italy), *Quat. Int.*, *122*, 7–30.